Title
Structural identification of a hotspot on CFTR for potentiation

Journal
Science, 364(6446)

ISSN
0036-8075

Authors
Liu, Fangyu
Zhang, Zhe
Levit, Anat
et al.

Publication Date
2019-06-21

DOI
10.1126/science.aaw7611

Peer reviewed

HHS Public Access

Author manuscript

Science. Author manuscript; available in PMC 2020 April 27.

Published in final edited form as:

Science. 2019 June 21; 364(6446): 1184–1188. doi:10.1126/science.aaw7611.

Structural identification of a hotspot on CFTR for potentiation

Fangyu Liu[1,2,*], **Zhe Zhang**[1,*], **Anat Levit**[3], **Jesper Levring**[1], **Kouki K. Touhara**[4,†], **Brian K. Shoichet**[3], **Jue Chen**[1,5,‡]

[1]Laboratory of Membrane Biophysics and Biology, The Rockefeller University, New York, NY 10065, USA.

[2]Tri-Institutional Training Program in Chemical Biology, The Rockefeller University, New York, NY 10065, USA.

[3]Department of Pharmaceutical Chemistry, University of California, San Francisco, San Francisco, CA 94158, USA.

[4]Laboratory of Molecular Neurobiology and Biophysics, The Rockefeller University, New York, NY 10065, USA.

[5]Howard Hughes Medical Institute, Chevy Chase, MD 20815, USA.

Abstract

Cystic fibrosis is a fatal disease caused by mutations in the cystic fibrosis transmembrane conductance regulator (CFTR). Two main categories of drugs are being developed: correctors that improve folding of CFTR and potentiators that recover the function of CFTR. Here we report two cryo–electron microscopy structures of human CFTR in complex with potentiators: one with the U.S. Food and Drug Administration (FDA)–approved drug ivacaftor at 3.3-angstrom resolution and the other with an investigational drug, GLPG1837, at 3.2-angstrom resolution. These two drugs, although chemically dissimilar, bind to the same site within the transmembrane region. Mutagenesis suggests that in both cases, hydrogen bonds provided by the protein are important for drug recognition.The molecular details of how ivacaftor and GLPG1837 interact with CFTR may facilitate structure-based optimization of therapeutic compounds.

‡**Corresponding author.** juechen@rockefeller.edu.

†Present address: Department of Physiology, University of California, San Francisco, CA 94143, USA.

Author contributions: F.L. and Z.Z. determined the cryo-EM structures of the CFTR–ivacaftor and CFTR–GLPG1837 complexes, respectively. F.L. performed the SPA assays. J.L. performed the bilayer experiments. F.L., Z.Z., and K.K.T. performed the patch-clamp experiments. A.L and B.K.S refined the structures of ivacaftor and GLPG1837 and performed the SAR analysis. J.C. conceptualized the study and analyzed the structures. J.C and F.L. wrote the manuscript with input from all authors.

*These authors contributed equally to the work.

Competing interests: The authors have no competing interests.

Data and materials availability: Cryo-EM density maps of the CFTR–drug complexes have been deposited in the Electron Microscopy Data Bank under the accession codes EMD-0611 (CFTR–Ivacaftor) and EMD-0606 (CFTR–GLPG1837). Atomic coordinates have been deposited in the Protein Data Bank under accession codes 6O2P (CFTR–Ivacaftor) and 6O1V (CFTR–GLPG1837). All data are available in the supplementary materials. This work is dedicated to the memory of David C. Gadsby.

SUPPLEMENTARY MATERIALS

science.sciencemag.org/content/[vol]/[issue]/[page]/suppl/DC1 Supplementary Text Materials and Methods Figs. S1 to S8 Tables S1 to S3 References (26–50)

The cystic fibrosis transmembrane conductance regulator (CFTR) is an anion channel widely expressed on epithelial surfaces of different organs, including the lung and intestine (1). It belongs to the family of the ATP-binding cassette (ABC) transporters, but functions as an anion channel. CFTR consists of two transmembrane domains (TMDs) that form the pore, two cytoplasmic nucleotide-binding domains (NBDs) that bind and hydrolyze adenosine 5′-triphosphate (ATP), and a regulatory (R) domain that must be phosphorylated to allow the channel to open (2). More than 300 mutations have been identified to cause cystic fibrosis (CF); details on the variants are given at the CFTR2 website (3). The most prevalent mutation is the deletion of a single amino acid, F508, which makes CFTR prone to degradation before reaching the cell's plasma membrane (4). Other mutants, such as E1371Q and G551D, are expressed on the cell membrane but do not gate properly (5).

Over the past eight decades, medical advances have improved the treatment of cystic fibrosis. The average survival age of patients has been lengthened from early infancy in the 1930s to around 47 years at present. Most treatments offer symptomatic relief, including pancreatic enzyme supplements to aid digestion, antibiotics to prevent and treat infection, mucus-thinning drugs to clear the airway, and lung transplants. Recently, therapies have been developed to target the CFTR protein. Small-molecule CFTR modulators include correctors that increase the abundance of CFTR at the cell surface and potentiators that increase the ion flux of mutant CFTR (6–8). Currently, two correctors (lumacaftor and tezacaftor) and one potentiator (ivacaftor), all developed by Vertex Pharmaceuticals, are available to patients (9–11). In addition, many other candidates to enhance the function of CFTR are in the drug discovery pipeline (7, 12, 13). All of these CFTR modulators were discovered through intensive high-throughput screening and iterative medicinal chemistry optimization. Rational drug discovery has not been feasible, owing to the lack of structural information. To address this issue, we report here cryo–electron microscopy (EM) structures of the human CFTR in complex with two different potentiators: the Vertex drug ivacaftor (6) and GLPG1837, an investigational drug developed by Galapagos (7).

Ivacaftor was discovered by screening compounds that increase anion flux in G551D-CFTR–expressing cells (6). Subsequent studies have shown that ivacaftor increases the open probability (P_O) of both wild-type (*wt*) and mutant CFTRs in membrane patches, proteoliposomes, and planar lipid bilayers (14–16). The potentiation by ivacaftor requires phosphorylation of CFTR by protein kinase A (PKA), but is independent of ATP (15). These results suggest that ivacaftor acts directly on CFTR, rather than functioning through other regulatory mechanisms.

To describe the specific molecular interactions between ivacaftor and CFTR, we determined a cryo-EM structure of ivacaftor in complex with phosphorylated E1371Q CFTR in the presence of saturating ATP-Mg^{2+} (10 mM) (Fig. 1A, figs. S1 to S3, and table S1). The final map has an overall resolution of 3.3 Å, showing well-defined density throughout the protein, except for the R domain. Density for both ATP-Mg^{2+} molecules are visible at the NBD dimer interface (fig. S3). An additional strong density is observed on the outer surface of the TMDs in the center of the lipid bilayer (Fig. 1C and fig S1C). This density, not observed in any of the previous CFTR structures (17–20), has a shape and size consistent with the chemical structure of ivacaftor (Fig. 1C and fig S3). Within this density, we built a model of

ivacaftor and examined multiple orientations of it in the site, using molecular docking (21, 22) followed by energy minimization of the proteinligand complex. Complexes were prioritized by their energetic complementarity, ability to make favorable polar interactions, and subsequent refinement to the electron density maps.

We previously reported the structure of the phosphorylated E1371Q construct in the presence of ATP-Mg^{2+} but in the absence of ivacaftor (20). The ivacaftor-bound E1371Q exhibits the same protein conformation in which the ATP-bound NBDs form a closed dimer, and the two TMDs pack closely together to form an ion conduction pathway open to the cytoplasmic solution. The R domain, largely unstructured, is located along the peripheral surface of NBD1 and the cytoplasmic region of the TMDs (Fig. 1A). No significant protein conformational changes were observed upon binding of ivacaftor, and the overall root mean square deviation between the two structures is 0.14 Å (Fig. 1B).

Ivacaftor binds CFTR at the protein-lipid interface, docking into a cleft formed by transmembrane (TM) 4, 5, and 8 (Fig. 1, C and D). The binding site coincides with a hinge region in TM8, a structural feature of CFTR not found in other ABC transporters (19, 20). The extracellular segment of TM 8 rotates around this hinge upon ATP binding (17–19); stabilizing this rotation may explain the drug's efficacy. Whereas about 40% of the molecular surface of ivacaftor is buried against CFTR, the remaining 60% is exposed to the hydrophobic region of the membrane (Fig. 1, C and D).

The interactions between ivacaftor and CFTR include two hydrogen bonds, two aromatic interactions, and six hydrophobic interactions (Fig. 2,A and B). To evaluate how each residue contributes to ivacaftor binding, we developed a scintillation proximity assay (SPA) to measure the apparent affinity of ivacaftor for CFTR (Fig. 2, C to E). Every residue in the binding site was individually substituted by alanine. Every mutant eluted from the size-exclusion column as a monomeric peak, similar to the *wt* CFTR, indicating that these mutations did not alter CFTR folding (fig. S4). Specific binding of ivacaftor to the *wt* CFTR increased as a function of ivacaftor concentration (Fig. 2C). Nonlinear regression analysis shows that the data fit well to a singlesite binding model with an equilibrium dissociation constant (K_d) of 6.6 ± 1.2 nM. In comparison, all but one mutation resulted in a reduced binding affinity for ivacaftor (Fig. 2, C to E, and table S2). Four residues appear to be most important—their alanine substitutions nearly abolishing ivacaftor binding (Fig. 2, C and D). Among them, S308 and F312 directly coordinate the oxoquinoline moiety through a hydrogen bond and a π- π stacking interaction, respectively (Fig. 2, A and B). The other two residues, R933 and Y304A, hydrogen bond to main-chain carbonyls in the TM 8 hinge, thus stabilizing the overall structure of the binding site (Fig. 2, A and B). Another important residue, F931, forms an edge-to-face interaction with the phenol ring of ivacaftor. Mutation of F931 to alanine decreased drug affinity by about 10-fold (Fig. 2D and table S2). Mutating F305, L233, and F236, the three residues within van der Waals distance from the oxoquinoline of the drug, also decreased its affinity (Fig. 2E and table S2). By contrast, substitution of F932, which interacts with one of the lipid-exposed tert-butyl groups, had no effect (Fig. 2E and table S2). These mutational effects are consistent with the structure of the CFTR–ivacaftor complex, indicating that hydrogen bonds are critical for ligand recognition in the low-dielectric environment of the membrane.

The structure of CFTR–ivacaftor complex largely explains the structure activity relationship (SAR) for the series of analogs that led to this drug (6). From the published SAR, 48 ivacaftor analogs, ranging from the initial high-throughput screening hit to optimized leads, may be readily docked into the ivacaftor site, making favorable interactions (fig. S5). The docked poses superpose with the ivafactor structure, recapitulating more and more of the the drug's interactions with CFTR as the molecules are optimized. Key interactions common to most of the docked complexes include the internal hydrogen bond between the conserved side-chain amide and the ubiquitous oxoquinoline oxygen, the hydrogen bond between the main-chain nitrogen of F931 and that same amide, and the interaction between the oxoquinoline nitrogen and S308. Similarly, the stacking observed between F312 and ivacaftor's oxoquinoline ring is conserved among the analogs. The phenolic hydroxyl, which appears late in the affinity maturation and is retained in ivacaftor, docks to interact with R933, as observed in the ivacaftor complex; addition of this group substantially increases affinity, at least partly reflecting its new interaction with the arginine (fig. S5; a more detailed analysis is presented in the supplementary text). These results are consistent with the ivafactor structure determined here and the SAR observed in its development (6).

Recently, a new potentiator, GLPG1837, has been discovered to have higher efficacy than that of ivacaftor (7). We first studied the effects of GLPG1837 in a planar bilayer system, where detergent-purified CFTR channels were reconstituted into liposomes then fused with a bilayer lipid membrane. At saturating ATP concentration, the P_o of the phosphorylated *wt* CFTR increased from 0.23 to 0.54 upon addition of 10 μM GLPG1837 (Fig. 3, A and B). The P_o of E1371Q was also increased by GLPG1837, from 0.64 to 0.88 (Fig. 3, A and B). The P_o values are lower than those measured in cellular membranes (23, 24), possibly owing to differences in their lipid compositions. Competitive binding assay shows that GLGP1837 reduced the apparent affinity of ivacaftor (Fig. 3C); the inhibition constant (K_i) was determined to be 0.30 ± 0.08 μM (Fig. 3D).

Next, we determined the cryo-EM structure of phosphorylated E1371Q CFTR in complex with ATP-Mg^{2+} and GLPG1837 (Fig. 3E, figs. S6 to S8, and table S3). The overall structure, at 3.2 Å resolution, is essentially indistinguishable from those of drug-free and ivacaftor-bound forms. Although GLPG1837 clearly binds in the same pocket, its orientation and shape differ from that of the ivacaftor density (Fig. 3F). Here too, a model of the CFTR–GLPG1837 complex was built by molecular docking, followed by energy minimization and refinement of the ligandreceptor complex. In the final model, the drug fits well into the electron density, with favorable polar and nonpolar interactions, and a relatively unstrained ligand geometry (Fig. 3F).

Although the chemical structure of GLPG1837 differs from that of ivacaftor, residues interacting with GLPG1837 largely overlap with those engaging ivacaftor (Fig. 4, A and B). Specifically, S308 and Y304 form hydrogen bonds; and L233, F236, F305, A309, F312 form hydrophobic interactions with the drug (Fig. 4, A and B). Four polar groups on GLPG1837 are engaged in intramolecular interactions (Fig. 4, A and B), also observed in the crystal structure of the compound itself (7), that shield charges, permitting this relatively polar molecule to permeate the membrane.

To evaluate the contribution of the intermolecular hydrogen bonds, we measured the halfmaximal effective concentration (EC_{50}) values of GLPG1837 for the *wt*, Y304A, and S308A CFTR (Fig. 4, C to E). The EC_{50} value of the *wt* CFTR was determined to be 0.12 ± 0.03 μM (Fig. 4C), similar to the reported value of 0.23 ± 0.12 mM (24). Replacing Y304 or S308 with an alanine increased the EC_{50} values by 57- and 34-fold, respectively (Fig. 4, D and E), underscoring the importance of the structurally observed hydrogen bonds in GLPG1837 recognition.

Here, we have described the structures of CFTR in complex with two separate potentiators. These structures allow us to reach several conclusions. First, although these two potentiators are chemically dissimilar, they both bind to the same site within the transmembrane region of CFTR. This explains why ivacaftor and GLPG1837 are competitive in electrophysiological and binding assays (Fig. 3, C and D) (24). Second, because the drug binding site coincides with a hinge involved in gating (19, 20), we propose that the presence of a drug in the pocket stabilizes the open configuration of the pore relative to the closed. In electrophysiological experiments, this stabilization is manifested as an increased opening rate and a decreased closing rate (Fig. 3A) (14, 25). The absence of observable protein structural differences between the drug-bound and drug-free conformations is not surprising given that an open probability increase from 0.64 to 0.88 (Fig. 3A) corresponds to a drug-induced energy change in the closed-open equilibrium (i.e., ΔΔG) of less than 2 k_BT (where k_B is the Boltzmann constant and T is temperature). Third, the drug-binding pocket identified here is likely a hotspot for the action of CFTR potentiators. It is now possible to use these structures of CFTR bound to two different potentiator molecules, together with computation, to identify new potentiators.

Supplementary Material

Refer to Web version on PubMed Central for supplementary material.

ACKNOWLEDGMENTS

We thank M. Ebrahim and J. Sotiris at Rockefeller's Evelyn Gruss Lipper Cryo-Electron Microscopy Resource Center for assistance in data collection and F. Glickman of the Rockefeller High-throughput and Spectroscopy Resource Center for help with the SPA experiments. We also thank P. Olinares and B. Chait for their mass spectrometry efforts to identify the density associated with R933, and D. Gadsby, R. MacKinnon, and T.-C. Hwang for advice on the electrophysiology experiments. Lastly, we thank C.-H. Lee and M. Lin for helpful discussions.

Funding: This work is supported by the Howard Hughes Medical Institute (to J.C), the Cystic Fibrosis Foundation Therapeutics (to J.C), the Charles H. Revson fellowship in Biomedical Science (to Z.Z), and R35GM122481 (to B.K.S).

REFERENCES AND NOTES

1. Elborn JS, Lancet 388, 2519–2531 (2016). [PubMed: 27140670]
2. Cheng SH et al., Cell 66, 1027–1036 (1991). [PubMed: 1716180]
3. https://www.cftr2.org/mutations_history
4. Cheng SH et al., Cell 63, 827–834 (1990). [PubMed: 1699669]
5. Welsh MJ, Smith AE, Cell 73, 1251–1254 (1993). [PubMed: 7686820]
6. Hadida S et al., J. Med. Chem 57, 9776–9795 (2014). [PubMed: 25441013]
7. Van der Plas SE et al., J. Med. Chem 61, 1425–1435 (2018). [PubMed: 29148763]

8. Van Goor F et al., Proc. Natl. Acad. Sci. U.S.A 108, 18843–18848 (2011). [PubMed: 21976485]
9. Taylor-Cousar JL et al., N. Engl. J. Med 377, 2013–2023 (2017). [PubMed: 29099344]
10. Wainwright CE et al., N. Engl. J. Med 373, 1783–1784 (2015).
11. Ramsey BW et al., N. Engl. J. Med 365, 1663–1672 (2011). [PubMed: 22047557]
12. Keating D et al., N. Engl. J. Med 379, 1612–1620 (2018). [PubMed: 30334692]
13. Davies JC et al., N. Engl. J. Med 379, 1599–1611 (2018). [PubMed: 30334693]
14. Jih KY, Hwang TC, Proc. Natl. Acad. Sci. U.S.A 110, 4404–4409 (2013). [PubMed: 23440202]
15. Eckford PD, Li C, Ramjeesingh M, Bear CE, J. Biol. Chem 287, 36639–36649 (2012). [PubMed: 22942289]
16. Van Goor F et al., Proc. Natl. Acad. Sci. U.S.A 106, 18825–18830 (2009). [PubMed: 19846789]
17. Liu F, Zhang Z, Csanády L, Gadsby DC, Chen J, Cell 169, 85–95.e8 (2017). [PubMed: 28340353]
18. Zhang Z, Chen J, Cell 167, 1586–1597.e9 (2016). [PubMed: 27912062]
19. Zhang Z, Liu F, Chen J, Cell 170, 483–491.e8 (2017). [PubMed: 28735752]
20. Zhang Z, Liu F, Chen J, Proc. Natl. Acad. Sci. U.S.A 115, 12757–12762 (2018). [PubMed: 30459277]
21. Coleman RG, Carchia M, Sterling T, Irwin JJ, Shoichet BK, PLOS ONE 8, e75992 (2013). [PubMed: 24098414]
22. Balius TE et al., Proc. Natl. Acad. Sci. U.S.A 114, E6839–E6846 (2017). [PubMed: 28760952]
23. Yu YC, Sohma Y, Hwang TC, J. Physiol 594, 3227–3244 (2016). [PubMed: 26846474]
24. Yeh HI, Sohma Y, Conrath K, Hwang TC, J. Gen. Physiol 149, 1105–1118 (2017). [PubMed: 29079713]
25. Grant T, Grigorieff N, eLife 4, e06980 (2015). [PubMed: 26023829]

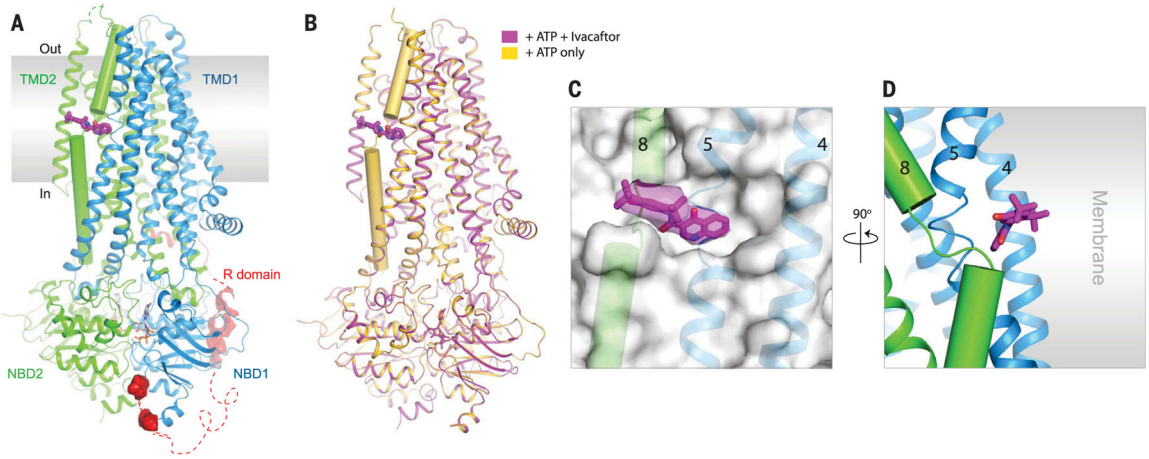

Fig. 1. Ivacaftor binds CFTR inside the membrane.

(**A**) Overall structure of the phosphorylated, ATP-bound human CFTR in complex with ivacaftor (shown in magenta). TMD1 and NBD1 are shown in blue, TMD2 and NBD2 in green, and R domain in red. TM8 is highlighted in cylinder representation. Regions not resolved in the structure are shown as dashed lines. (**B**) Superposition of phosphorylated, ATP-bound CFTR in the absence (yellow) and presence of ivacaftor (magenta). (**C**) A magnified view of the ivacaftor-binding site. CFTR is shown as a transparent surface model with TM 4, 5, and 8 indicated. Ivacaftor is shown as a stick model together with the corresponding EM density. (**D**) Ivacaftor binds at the protein-lipid interface, exposing half of its surface to the lipid bilayer.

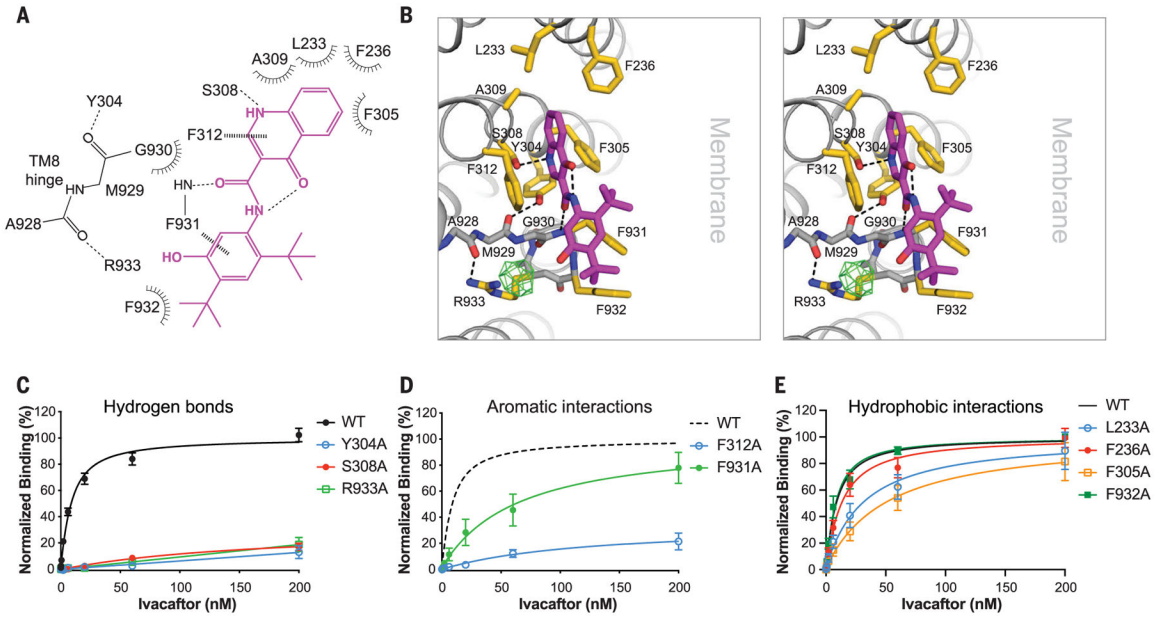

Fig. 2. Contribution of individual residues to ivacaftor binding.

(**A**) Schematic drawing of interactions formed between ivacaftor (magenta) and the CFTR-binding site. Residues within van der Waals distances (<4.5 Å) are shown. Representations: black dashed lines, hydrogen bonds; blue vertical lines, aromatic interactions; spokes, hydrophobic interactions. The hinge region in TM8 is shown as gray sticks and labeled. (**B**) Stereo view of the ivacaftor-binding site. Residues within van der Waals distances are shown in yellow, and hydrogen bonds are depicted as black dashed lines. An unknown density between R933 and ivacaftor is shown as green mesh. (**C** to **E**) Binding affinities of *wt* CFTR and mutants replacing residues making (**C**) hydrogen bonds, (**D**) aromatic interactions, and (**E**) hydrophobic interactions with ivacaftor. Data points represent the means and SEMs of at least three measurements. The calculated K_d values are listed in Table S2. Single-letter abbreviations for the amino acid residues are as follows: A, Ala; D, Asp;E, Glu; F, Phe; G, Gly; L, Leu; M, Met; Q, Gln R, Arg; S, Ser; and Y, Tyr.

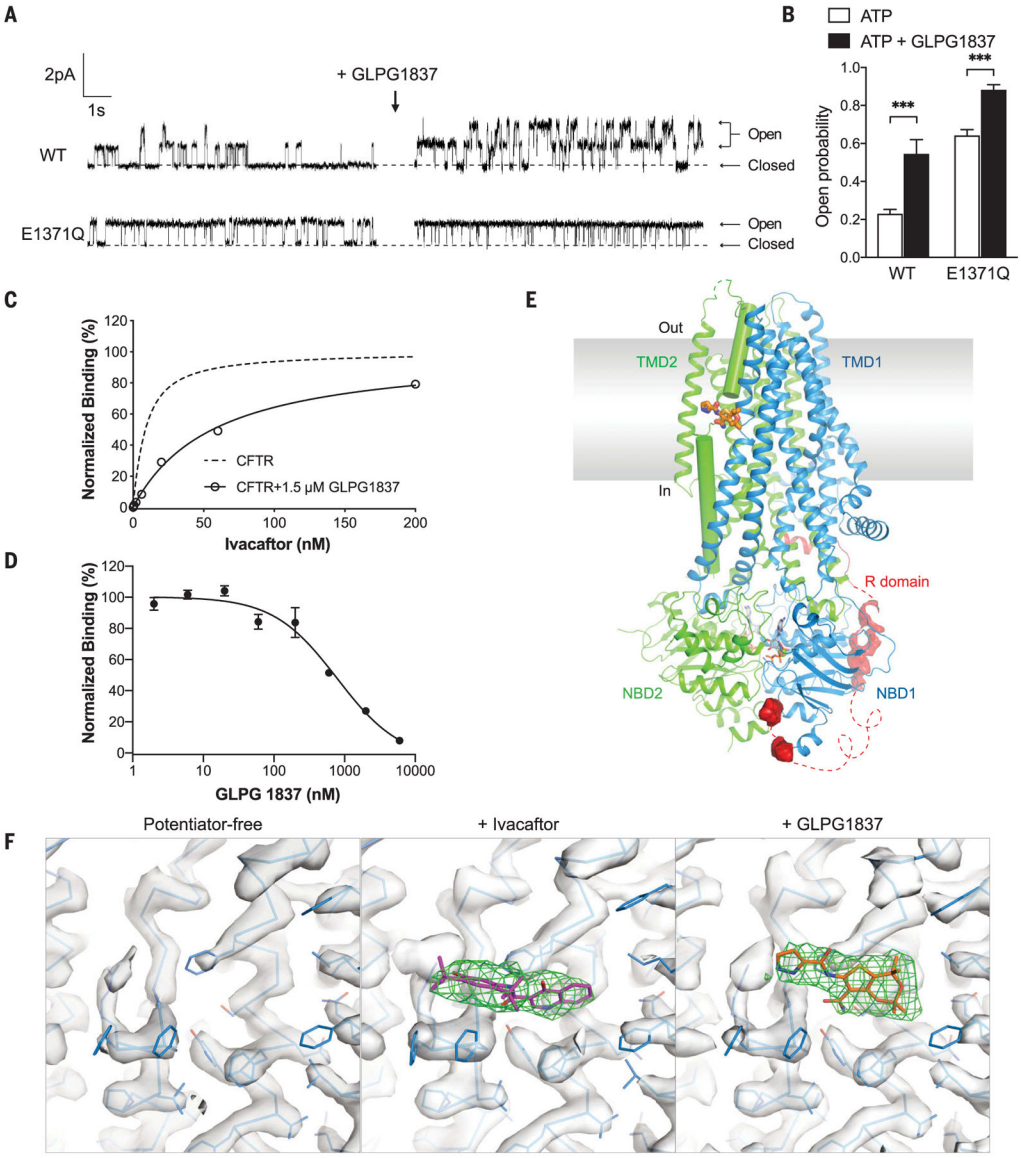

Fig. 3. GLPG1837 binds to the same site as ivacaftor.

(**A**) Representative recordings of *wt* (upper trace) and E1371Q (lower trace) CFTR reconstituted in synthetic lipid bilayers. CFTR was phosphorylated with PKA prior to fusion with bilayers. Recordings were performed on individual membranes with 2 mM ATP before (left) and after (right) addition of 10 μM GLPG1837. (**B**) Open probabilities of *wt* and E1371Q CFTR before (open bar) and after (filled bar) addition of 10 μM GLPG1837. Data points represent the means and SEMs. P_o = 0.23 ± 0.02, n = 9, for *wt*; P_o = 0.54 ± 0.08, n = 3, for *wt* + GLPG1837; P_o = 0.64 ± 0.03, n = 7, for E1371Q; P_o = 0.88 ± 0.03, n = 6, for E1371Q + GLPG1837. (**C**) The presence of 1.5 μM GLPG1837 shifts the apparent K_d of ivacaftor from 6.6 ± 1.2 nM (dashed line) to 54 ± 4 nM (solid line, n = 9). (**D**) Competition binding assay. Ivacaftor was kept at a constant concentration of 8 nM, and its binding to wt CFTR is plotted as a function of GLPG1837 concentration. K_i = 0.30 ± 0.08 μM. (**E**) Ribbon diagram of the phosphorylated, ATP-bound CFTR in complex with GLPG1837 (stick

representation, orange). (**F**) EM density at the potentiator-binding site in the potentiator-free (left), ivacaftor-bound (center), and GLPG1837-bound (right) reconstructions. Densities corresponding to CFTR are shown in gray, whereas densities only observed in the potentiator-bound maps are shown as green meshes. All maps are contoured at 9σ.

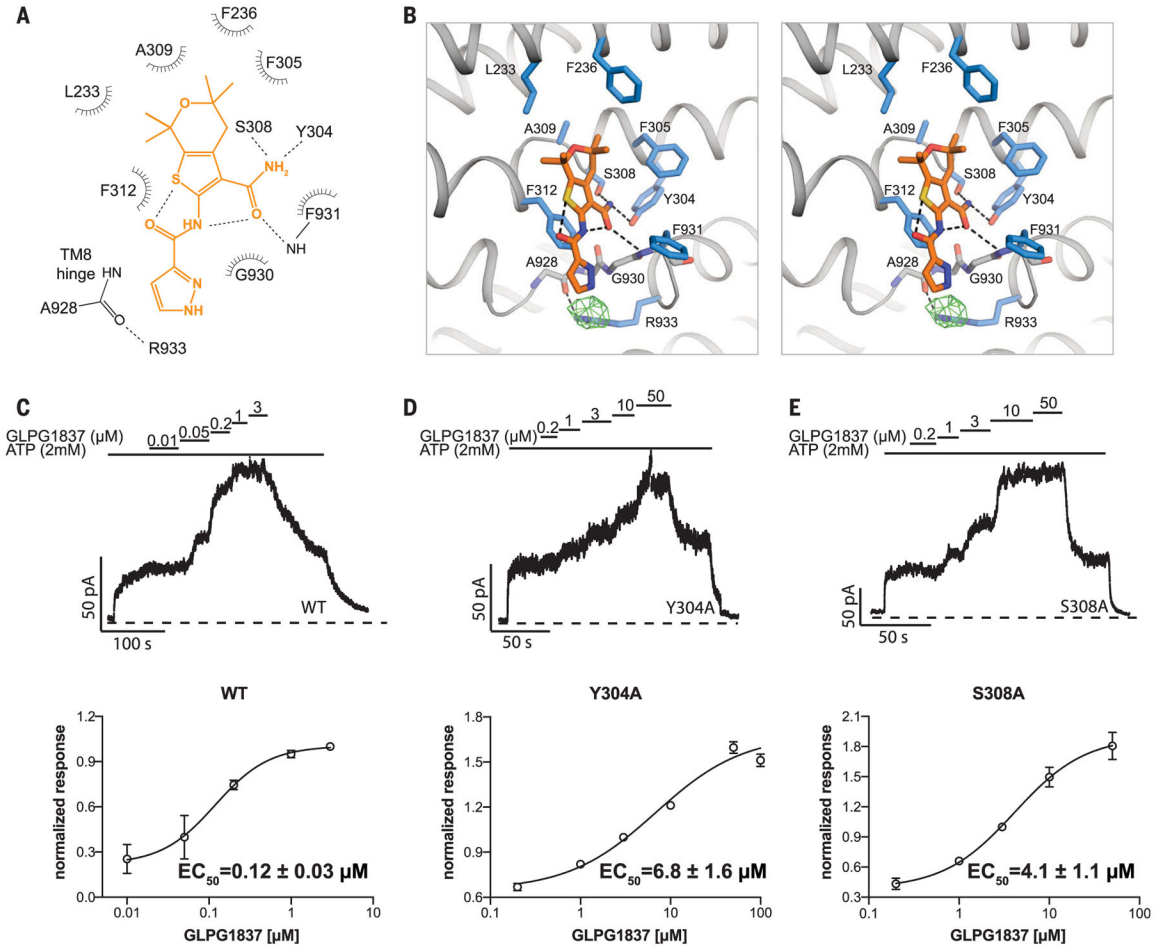

Fig. 4. Molecular details of GLPG1837 binding.

(**A**) Schematic drawing of the interactions between GLPG1837 (orange) and CFTR. Hydrogen bonds are represented by black dashed lines, and hydrophobic interactions are shown by the spokes. (**B**) Stereo view of the GLPG1837 binding site. Residues within van der Waals distances (<4.5 Å) are shown as blue sticks, and hydrogen bonds are depicted as black dashed lines. An unknown density between R933 and GLPG1837 is shown in green mesh. (**C** to **E**) Upper panel: Representative macroscopic current traces of *wt* and mutant CFTR in response to GLPG1837 perfusion. Different concentrations of GLPG1837 applied after channel activation are marked above the trace. Lower panel: Dose-response curves with estimated EC_{50} values. CFTR-containing membrane patches were fully phosphorylated by PKA in the presence of saturating amount of ATP before GLPG1837 titration. The total current at 3 μM GLPG1837 was used to normalize the current potentiated by different concentrations of GLPG1837. The dose responses were fitted with the Hill equation. Each data point represents values determined from five to nine patches.